UNIVERSAL WISER
PUBLISHER

Research Article

Gap Dromions and Domain Walls with Dispersive Reflectivity Having Cubic-Quintic-Septic-Nonic Self-Phase Modulation in Presence of Multiplicative White Noise

E. M. E. Zayed[1], Khaled A. E. Alurrfi[2], Manar S. Ahmed[3], Ahmed H. Arnous[4,5], Yakup Yildirim[6,7*], Luminita Moraru[8,9], Amer Shaker Mahmood[10], Ibrahim Zegalhaiton Chaloob[11], Farag Mahel Mohammed[12], Anjan Biswas[13,14,15,16]

[1]Department of Mathematics, Faculty of Science, Zagazig University, Zagazig, Egypt
[2]Department of Mathematics, Faculty of Science, Elmergib University, Khoms, Libya
[3]Department of Engineering Mathematics and Physics, Higher Institute of Engineering, El-Shorouk Academy, Cairo, Egypt
[4]Department of Mathematical Sciences, Saveetha School of Engineering, SIMATS, Chennai, Tamilnadu, 602105, India
[5]Research Center of Applied Mathematics, Khazar University, Baku, AZ, 1096, Azerbaijan
[6]Department of Computer Engineering, Biruni University, Istanbul, 34010, Turkey
[7]Mathematics Research Center, Near East University, Nicosia, 99138, Cyprus
[8]Department of Chemistry, Physics and Environment, Faculty of Sciences and Environment, Dunarea de Jos University of Galati, 47 Domneasca Street, Galati, 800008, Romania
[9]Department of Physics, Sefako Makgatho Health Sciences University, Medunsa, 0204, South Africa
[10]Medical Laboratory Techniques Department, College of Medical and Health Technologies, Al-Nibras University, Tikrit, 34001, Iraq
[11]Department of Business Administration, College of Administration and Economics, Al-Esraa University, Baghdad, 10069, Iraq
[12]Al-Nibras University, Tikrit, 34001, Iraq
[13]Department of Mathematics and Physics, Grambling State University, Grambling, LA, 71245-2715, USA
[14]Department of Physics and Electronics, Khazar University, Baku, AZ, 1096, Azerbaijan
[15]Department of Applied Sciences, Cross-Border Faculty of Humanities, Economics and Engineering, Dunarea de Jos University of Galati, 111 Domneasca Street, Galati, 800201, Romania
[16]Department of Mathematics and Applied Mathematics, Sefako Makgatho Health Sciences University, Medunsa, 0204, South Africa
 E-mail: yyildirim@biruni.edu.tr

Abstract: This paper is about the retrieval of gap dromions in presence of multiplicative white noise. The self-phase modulation structure is with cubic-quintic-septic-nonic structure. Two integration approaches retrieve the dromions and domain walls with the usage of the enhanced direct algebraic approach and the addendum to Kudryashov's scheme. The solutions are subsequently classified.

Keywords: dromions, Bragg gratings, integrability

1. Introduction

One of the critical challenges in optical soliton transmission over transcontinental and transoceanic distances lies in preserving the delicate balance between Chromatic Dispersion (CD) and Self-Phase Modulation (SPM). This equilibrium is essential for the stable propagation of optical solitons. When disrupted, it can lead to wave collapse, resulting in severe degradation of signal quality and potentially catastrophic consequences for communication systems. To address this issue, several theoretical and practical countermeasures have been developed within the field of fiber optic dynamics [1–5].

Among the theoretical strategies, the incorporation of higher-order dispersive effects such as spatio-temporal dispersion and the consideration of advanced soliton forms, including cubic-quartic and highly dispersive solitons, have shown promise. On the engineering front, a particularly notable solution is the implementation of Bragg gratings. These structures effectively replace the role of CD with dispersive reflectivity, thereby mitigating the depletion of dispersion over long-haul transmissions. This advancement has been successfully realized by telecommunications engineers and represents a significant leap in optical fiber technology [6–10].

In a Bragg-grating configuration, the periodic modulation of the refractive index induces dispersive reflectivity and opens a spectral bandgap that can support exponentially localized modes known as gap solitons or, in two spatial dimensions, gap dromions. Within this framework, dromions are localized in both transverse coordinates (x, y) and evolve along the propagation direction, representing a higher-dimensional analogue of one-dimensional optical solitons. In contrast, domain walls arise as heteroclinic fronts connecting two distinct steady states permitted by the nonlinear medium.

The present work extends this framework by incorporating a generalized SPM nonlinearity consisting of cubic, quintic, septic, and nonic terms. This extended nonlinear profile allows the model to capture complex nonlinear responses encountered in high-intensity optical media and advanced fiber systems [11–15]. To further align the model with realistic physical environments, we introduce multiplicative white noise to represent stochastic fluctuations in system parameters such as refractive index or grating strength [16–20]. This addition transforms the governing deterministic equation into a Stochastic Nonlinear Schrödinger Equation (SNLSE), thereby enabling the exploration of noise-induced effects on localized wave structures.

Two analytical techniques are employed to retrieve explicit localized solutions: the enhanced direct algebraic method and an addendum to Kudryashov's approach [21–25]. These integration schemes yield exact gap dromion and domain wall configurations, which are systematically classified according to their structure and dynamical characteristics. The findings enrich the theoretical understanding of stochastic optical solitons and provide potential implications for the design and stabilization of next-generation fiber-optic communication systems.

The motivation behind this work stems from the growing need to understand the stability and dynamics of localized optical structures in realistic nonlinear media, where both high-order nonlinear effects and stochastic fluctuations coexist. While classical studies of solitons in Kerr-type (cubic) media have provided valuable insights, modern optical systems, such as high-intensity fiber lasers, photonic crystal fibers, and Bragg-grating-based transmission lines—operate in regimes where higher-order nonlinearities (quintic, septic, and nonic) become non-negligible. Moreover, environmental and fabrication-induced fluctuations introduce stochasticity that can significantly affect soliton robustness and coherence. Therefore, a comprehensive model that simultaneously incorporates dispersive reflectivity, multi-order self-phase modulation, and multiplicative white noise is essential to capture these realistic conditions. The present study is motivated by this gap, aiming to provide exact analytical solutions and a systematic classification of gap dromions and domain walls in such stochastic, strongly nonlinear optical environments.

1.1 *Governing model*

In this work, we introduce, for the first time, the stochastic $(2 + 1)$-dimensional perturbed Nonlinear Schrödinger Equation (NLSE) that models the complex dynamics of optical pulse propagation in fiber Bragg gratings. This advanced model incorporates the combined effects of higher-order nonlinearities specifically, cubic, quintic, septic, and nonic nonlinear terms which reflect the nonlinear response of the optical medium to high-intensity light. The cubic nonlinearity corresponds to the standard Kerr effect, where the refractive index of the fiber varies linearly with the optical intensity.

The quintic term accounts for fifth-order susceptibility contributions, which become significant at higher field intensities and serve to stabilize or destabilize pulse dynamics, depending on their sign. The septic (seventh-order) and nonic (ninth-order) nonlinearities capture even higher-order interactions, offering a more accurate and comprehensive representation of the nonlinear refractive index variation in strongly nonlinear or highly confined optical media, such as those used in photonic crystal fibers or engineered Bragg gratings. Moreover, the model explicitly incorporates stochastic perturbations in the form of multiplicative white noise, which is a realistic representation of random fluctuations due to environmental variations, manufacturing imperfections, or quantum noise sources. These random effects are mathematically treated in the Itô calculus framework, which is well-suited for analyzing systems affected by noise, particularly when the noise intensity depends on the system state (i.e., is multiplicative in nature). The $(2 + 1)$-dimensional structure of the model indicates that it accounts for the evolution of the optical field along the propagation direction (typically denoted as the longitudinal axis) while also incorporating transverse spatial variations and temporal evolution, thus providing a richer and more physically realistic description of pulse dynamics in multidimensional settings.

The equation derived and presented here is therefore a significant generalization of the standard NLSE, and it has not previously appeared in the literature in this comprehensive dimensionless stochastic form that unifies multi-order nonlinearity, and multiplicative noise. The full form of this novel equation is given as follows:

$$iq_t + a_1 (r_{xx} + r_{yy}) + \left[e_1 |q|^2 + k_1 |r|^2\right] q + \left[l_1 |q|^4 + m_1 |q|^2 |r|^2 + n_1 |r|^4\right] q + \left[p_1 |q|^6 + q_1 |q|^2 |r|^4 + r_1 |q|^4 |r|^2\right.$$

$$\left. + s_1 |r|^6\right] q + \left[\zeta_1 |q|^8 + \eta_1 |q|^2 |r|^6 + \gamma_1 |q|^6 |r|^2 + \sigma_1 |q|^4 |r|^4 + \Sigma_1 |r|^8\right] q + \sigma q \frac{dW(t)}{dt} + i\alpha_1 q_x + \beta_1 r + \delta_1 q^* r^2$$

$$= i \left[\mu_1 \left(|q|^2 q\right)_x + \theta_1 \left(|q|^2\right)_x q + \nu_1 |q|^2 q_x\right], \tag{1}$$

$$ir_t + a_2 (q_{xx} + q_{yy}) + \left[e_2 |r|^2 + k_2 |q|^2\right] r + \left[l_2 |r|^4 + m_2 |r|^2 |q|^2 + n_2 |q|^4\right] r + \left[p_2 |r|^6 + q_2 |r|^2 |q|^4 + q_2 |r|^4 |q|^2\right.$$

$$\left. + s_2 |q|^6\right] r + \left[\zeta_2 |r|^8 + \eta_2 |r|^2 |q|^6 + \gamma_2 |r|^6 |q|^2 + \sigma_2 |r|^4 |q|^4 + \Sigma_2 |q|^8\right] r + \sigma r \frac{dW(t)}{dt} + i\alpha_2 r_x + \beta_2 q + \delta_2 r^* q^2$$

$$= i \left[\mu_2 \left(|r|^2 r\right)_x + \theta_2 \left(|r|^2\right)_x r + \nu_2 |r|^2 r_x\right]. \tag{2}$$

In the present analysis, the functions $q(x, y, t)$ and $r(x, y, t)$ are defined as complex-valued wave fields that describe the spatiotemporal evolution of the optical pulse envelopes in a coupled system. These functions encapsulate both the amplitude and phase information of the propagating optical waves in two transverse spatial dimensions x and y, and time t. Their respective complex conjugates, $q^*(x, y, t)$ and $r^*(x, y, t)$, appear throughout the equations to account for nonlinear interactions that involve both self- and cross-phase modulations, as well as higher-order nonlinear coupling. Here, the imaginary unit i is defined as the square root of negative one, $i = \sqrt{-1}$, as is standard in complex-valued wave equations. The leading terms in equations (1) and (2) represent the linear evolution of the wave functions in time, typically denoted by iq_t and ir_t, and describe the natural temporal progression of the optical wave packets in the absence of dispersion and nonlinear effects. These temporal derivatives establish the baseline behavior of the system and are foundational to understanding the modifications introduced by dispersion, nonlinearity, and stochasticity. The parameters a_j (with $j = 1, 2$) serve as the CD coefficients in the x- and y-directions, respectively. CD refers to the wavelength-dependent spread of the pulse as it propagates, and the inclusion of these terms in both spatial directions reflects the two-dimensional

character of the optical field evolution, which is essential for modeling beam-like or planar waveguide geometries, such as in fiber Bragg gratings or nonlinear planar waveguides. The parameters e_j, l_j, p_j, ζ_j (for $j = 1, 2$) represent the coefficients of the SPM terms of various orders. SPM arises due to the intensity-dependent change in the refractive index of the medium, which affects the phase of the propagating wave. These coefficients govern the strength of nonlinear phase shifts introduced by the optical field's own intensity, with each coefficient typically associated with a specific nonlinear power law (e.g., cubic, quintic, septic, nonic). The constants k_j, m_j, n_j, q_j, r_j, s_j, η_j, γ_j, σ_j, Σ_j (again with $j = 1, 2$) define the strengths of Cross-Phase Modulation (XPM) interactions. XPM is a nonlinear effect where the intensity of one optical field induces a phase shift in another co-propagating field. These coefficients capture the influence of inter-modal or inter-channel nonlinearities, and are essential for modeling coupled field dynamics, especially in multi-mode systems, birefringent fibers, or systems with interacting polarization components. The parameter σ denotes the noise intensity coefficient, which quantifies the strength of the stochastic perturbation acting on the system. The stochastic component is introduced through the Wiener process $W(t)$, a standard mathematical model for Brownian motion. The temporal derivative $dW(t)/dt$ formally corresponds to white noise—a zero-mean, delta-correlated random process. In this context, the noise is multiplicative, meaning its effect depends on the amplitude of the field, and it is interpreted in the sense of Itô calculus, which is appropriate for rigorous treatment of such stochastic differential equations. The terms with coefficients α_j, β_j, τ_j, δ_j (with $j = 1, 2$) represent various physical effects that further enrich the model. Specifically α_j and β_j account for Inter-Modal Dispersion (IMD), which describes the differential temporal spreading of coupled modes. τ_j incorporates detuning effects, which reflect the deviation of the operating frequency from resonance. δ_j captures the influence of four-Wave Mixing (4WM), a nonlinear interaction among four wave components that can lead to energy transfer and spectral broadening. Finally, the coefficients μ_j, θ_j, ν_j (again indexed by $j = 1, 2$) are associated with higher-order nonlinear phenomena such as self-steepening and nonlinear dispersion. The self-steepening effect results from intensity-dependent group velocity and leads to pulse distortion and spectral broadening. Nonlinear dispersion accounts for variations in group velocity dispersion due to high field strengths. Together, these effects allow the model to capture intricate details of pulse propagation, including shock formation and asymmetry in pulse shapes.

Equations (1)-(2) represent the coupled nonlinear Schrödinger equations in $(2 + 1)$ dimensions for counterpropagating optical fields in a Bragg grating with dispersive reflectivity. They include cubic, quintic, septic, and nonic self and cross phase modulation terms to describe higher-order nonlinear interactions beyond the Kerr approximation [26, 27]. The formulation is consistent with recent studies on $(2 + 1)D$ optical systems that incorporate high-order nonlinear effects and stochastic perturbations governed by multiplicative white noise within the Itô framework [28, 29]. The stochastic components account for random fluctuations in the fields and system parameters, reflecting realistic noisy Bragg structures.

The goal of this study is to systematically analyze the coupled stochastic nonlinear Schrödinger equations (1) and (2) by applying two powerful analytical techniques: the enhanced direct algebraic method and the extended Kudryashov method. These methods are particularly suited for constructing exact or approximate traveling wave solutions, allowing for the classification and characterization of solitary wave profiles under the influence of high-order nonlinearities and stochastic fluctuations.

This work provides, to the best of our knowledge, the first analytical treatment of $(2+1)D$ gap dromions and domain walls in Bragg-grating media with dispersive reflectivity under multiplicative white noise, while retaining a high-order Self-Phase Modulation (SPM) structure comprising cubic, quintic, septic, and nonic nonlinearities. A two-track integration framework is developed, combining the enhanced direct algebraic and extended Kudryashov approaches, which together yield closed-form families of localized solutions in this stochastic and strongly nonlinear setting. The retrieved solutions are systematically classified with respect to their existence conditions, localization lengths, amplitude-phase structures, and parameter interdependencies, explicitly revealing how noise and higher-order nonlinearities influence the solution manifolds. Furthermore, the analysis connects these solutions to limiting regimes such as noiseless and lower-order SPM truncations, demonstrating that the new families generalize and extend known deterministic results in dispersively reflective media. Collectively, these contributions establish the originality and significance of the paper relative to prior studies on deterministic Kerr or low-order models without stochasticity.

We adopt two complementary analytic routes, the enhanced direct algebraic approach and an addendum to Kudryashov's scheme, because the governing $(2+1)D$ model exhibits a balanceable polynomial structure: dispersive reflectivity (Bragg coupling) and self-phase modulation with cubic-quintic-septic-nonic terms. These methods exploit algebraic balance to yield closed-form localized solutions and, crucially, make explicit how coefficients (including multiplicative-noise intensities and coupling factors) enter the amplitude, phase, and localization parameters. Using both routes provides cross-validation: each independently retrieves families of gap dromions and domain walls with consistent parameter constraints, thereby strengthening correctness and interpretability of the obtained solution classes.

2. Mathematical preliminaries

In order to derive solutions to equations (1) and (2), we introduce an ansatz for the wave profiles that simplifies the complex equations by assuming the form of traveling wave solutions. The wave profiles for $q(x, y, t)$ and $r(x, y, t)$ are assumed to have the following general forms:

$$q(x, y, t) = \phi(\xi) \exp\left[i\left(-\kappa_1 x - \kappa_2 y + (\omega - \sigma^2)t + \sigma W(t)\right)\right], \qquad (3)$$

$$r(x, y, t) = \psi(\xi) \exp\left[i\left(-\kappa_1 x - \kappa_2 y + (\omega - \sigma^2)t + \sigma W(t)\right)\right], \qquad (4)$$

$$\xi = \rho_1 x + \rho_2 y - ct. \qquad (5)$$

Here, κ_j, ρ_j, ω, c, and σ are real constants, each serving a specific role in the dynamics of the system. κ_1 and κ_2 are wavevector components in the x- and y-directions, respectively, representing the spatial frequency of the wave in each direction. ω is the central frequency of the wave, determining the oscillatory nature of the wave in time. c represents the velocity of the traveling wave, which links the spatiotemporal coordinates via the similarity variable ξ. σ is the noise intensity coefficient, which modulates the strength of the random fluctuations described by the Wiener process $W(t)$. The terms $\phi(\xi)$ and $\psi(\xi)$ are real-valued functions, which represent the envelope profiles of the wavefunctions $q(x, y, t)$ and $r(x, y, t)$, respectively. These functions characterize the shape and evolution of the optical pulses as they propagate through the medium. The variable ξ is a moving frame variable that describes the transformation from the Cartesian coordinates x, y, and time t to a reference frame that moves with the wave at velocity c. The coefficients ρ_1 and ρ_2 are related to the direction of wave propagation in the x- and y-directions, respectively. These coefficients are chosen such that the combined motion of the wave can be described in terms of the evolution along a generalized direction, accounting for the multi-dimensionality of the wave propagation. The exponential factors in equations (3) and (4) account for the oscillatory behavior of the waves in time and space. The term $-\kappa_1 x - \kappa_2 y$ represents the spatial phase evolution of the waves in the x- and y-directions, while the term $(\omega - \sigma^2)t$ represents the temporal evolution of the phase, where ω is the central frequency of the wave and σ^2 modifies this frequency due to the noise effect. The factor $\sigma W(t)$ introduces the stochastic perturbations via the Wiener process $W(t)$, which models the random fluctuations in the system.

By substituting the wave profiles $q(x, y, t)$ and $r(x, y, t)$ as given in equations (3) and (4) into the original equations (1) and (2), we obtain a system of equations that is easier to handle analytically. Specifically, the substitution allows us to separate the resulting equations into their real and imaginary parts, which significantly simplifies the problem by transforming the original coupled complex equations into a system of real-valued ordinary differential equations. These equations are essential for further analysis, as they determine the stability and dynamics of the solitons under the influence of higher-order nonlinearities and stochastic effects. The real parts of these equations correspond to the evolution of the wave envelopes $\phi(\xi)$ and $\psi(\xi)$, which govern the intensity and shape of the optical pulses:

$$\left[\left(\rho_1^2+\rho_2^2\right)a_1\right]\psi''+\zeta_1\phi^9+\left(\gamma_1\psi^2+p_1\right)\phi^7+\left(\sigma_1\psi^4+r_1\psi^2+l_1\right)\phi^5$$

$$+\left[\eta_1\psi^6+q_1\psi^4+m_1\psi^2-(\mu_1+\nu_1)\kappa_1+e_1\right]\phi^3+\left[\Sigma_1\psi^8+s_1\psi^6+n_1\psi^4+(k_1+\delta_1)\psi^2+\alpha_1\kappa_1+\sigma^2-\omega\right]\phi$$

$$+\left[\left(\omega-\sigma^2\right)b_1\kappa_1-\left(\kappa_1^2+\kappa_2^2\right)a_1+\beta_1\right]\psi=0, \tag{6}$$

and

$$\left[\left(\rho_1^2+\rho_2^2\right)a_2\right]\phi''+\zeta_2\psi^9+\left(\gamma_2\phi^2+p_2\right)\psi^7+\left(\sigma_2\phi^4+r_2\phi^2+l_2\right)\psi^5$$

$$+\left[\eta_2\phi^6+q_2\phi^4+m_2\phi^2-(\mu_2+\nu_2)\kappa_1+e_2\right]\psi^3+\left[\Sigma_2\phi^8+s_2\phi^6+n_2\phi^4+(k_2+\delta_2)\phi^2+\alpha_2\kappa_1+\sigma^2-\omega\right]\psi$$

$$+\left[\left(\omega-\sigma^2\right)b_2\kappa_1-\left(\kappa_1^2+\kappa_2^2\right)a_2+\beta_2\right]\phi=0. \tag{7}$$

The imaginary parts are derived by isolating the terms involving the imaginary unit i in the complex exponential expressions of the wave profiles $q(x,y,t)$ and $r(x,y,t)$, which were previously assumed in equations (3) and (4). The imaginary parts of these expressions correspond to the phase evolution of the waves, encapsulating the dynamic behavior and interaction of the wave functions in the complex plane:

$$-2\rho_1\kappa_1a_1-2\kappa_2a_1\rho_2-\rho_1\left(\nu_1+2\theta_1+3\mu_1\right)\phi^2\phi'+\left(\rho_1\alpha_1-c\right)\phi'=0, \tag{8}$$

and

$$-2\rho_1\kappa_1a_2-2\kappa_2a_2\rho_2-\rho_1\left(\nu_2+2\theta_2+3\mu_2\right)\psi^2\psi'+\left(\rho_1\alpha_2-c\right)\psi'=0. \tag{9}$$

To make the subsequent steps simpler, we introduce a substitution to simplify the expressions. Specifically, we define a new function $\psi(\xi)$ as follows:

$$\psi(\xi)=H\phi(\xi), \tag{10}$$

where H is a nonzero constant. This substitution allows us to express the variable $\psi(\xi)$ in terms of the function $\phi(\xi)$, scaled by a constant factor H. Now that we have made this substitution, we can revisit the two equations (6) and (7). These equations, which involve the function $\psi(\xi)$, will be simplified by the substitution. The effect of this substitution on the equations is as follows. By substituting $\psi(\xi)=H\phi(\xi)$ into both equations (6) and (7), the equations will be reduced to simpler forms that involve only the function $\phi(\xi)$ and the constant H, rather than the function $\psi(\xi)$ directly:

$$\left[\left(\rho_1^2 + \rho_2^2 \right) a_1 \right] H \phi'' + \left(H^4 n_1 + H^2 m_1 + l_1 \right) \phi^5 + \left(H^6 s_1 + H^4 q_1 + H^2 r_1 + p_1 \right) \phi^7$$

$$+ \left[H^8 \Sigma_1 + H^6 \eta_1 + H^4 \sigma_1 + H^2 \gamma_1 + \zeta_1 \right] \phi^9 + \left[(k_1 + \delta_1) H^2 - (\mu_1 + \nu_1) \kappa_1 + e_1 \right] \phi^3$$

$$+ \left[\beta_1 H + \alpha_1 \kappa_1 - \left(\kappa_1^2 + \kappa_2^2 \right) H a_1 + \sigma^2 - \omega \right] \phi = 0, \tag{11}$$

and

$$\left[\left(\rho_1^2 + \rho_2^2 \right) a_2 \right] \phi'' + H \left(H^4 l_2 + H^2 m_2 + n_2 \right) \phi^5 + H \left(H^6 p_2 + H^4 r_2 + H^2 q_2 + s_2 \right) \phi^7$$

$$+ H \left[H^8 \zeta_2 + H^6 \gamma_2 + H^4 \sigma_2 + H^2 \eta_2 + \Sigma_2 \right] \phi^9 + \left[(e_2 - (\mu_2 + \nu_2) \kappa_1) H^2 + k_2 + \delta_2 \right] H \phi^3$$

$$+ \left[\left(\sigma^2 + \alpha_2 \kappa_1 - \omega \right) H - \left(\kappa_1^2 + \kappa_2^2 \right) a_2 + \beta_2 \right] \phi = 0. \tag{12}$$

These reduced forms will allow us to work with more manageable expressions for the next steps in the analysis. The general goal of this step is to transform the original equations into forms that are easier to handle by reducing the number of variables or by simplifying the structure of the equations. Similarly, equations (8) and (9) can be converted to:

$$\left[\left(-2 a_1 \kappa_1 \rho_1 - 2 \rho_2 \kappa_2 a_1 \right) H + \rho_1 \alpha_1 - c \right] \phi' - \rho_1 \left(\nu_1 + 2\theta_1 + 3\mu_1 \right) \phi^2 \phi' = 0, \tag{13}$$

and

$$\left[-2 a_2 \kappa_1 \rho_1 - 2 \rho_2 \kappa_2 a_2 + \left(\rho_1 \alpha_2 - c \right) H \right] \phi' - \rho_1 \left(\nu_2 + 2\theta_2 + 3\mu_2 \right) H^3 \phi^2 \phi' = 0. \tag{14}$$

We are now considering the application of the principle of linear independence to equations (13) and (14). This principle can be applied in various mathematical contexts, including the analysis of solutions to systems of equations. When we apply the principle of linear independence to the equations (13) and (14), it means that we assume that the terms involved in these equations are linearly independent. By doing this, we derive specific relationships between the parameters, as shown in the following equations:

$$\begin{cases} c = -2 H a_1 \kappa_1 \rho_1 - 2 H a_1 \kappa_2 \rho_2 + \rho_1 \alpha_1, \\ \\ c = \dfrac{+ H \alpha_2 \rho_1 - 2 a_2 \kappa_1 \rho_1 - 2 \rho_2 \kappa_2 a_2}{-H}, \end{cases} \tag{15}$$

These equations represent specific expressions for the constant c derived from the linear independence of the terms involved in equations (13) and (14). The first equation provides a relationship that incorporates various parameters such as H, a_1, κ_1, κ_2, ρ_1, and α_1. The second equation similarly expresses c in terms of other parameters, including H, a_2, α_2, ρ_1, and ρ_2. These equations are not arbitrary, but are derived from ensuring that the terms in the original equations (13) and (14) are linearly independent. This leads to the relationships above, which allow us to solve for c in terms of other known variables and constants. In addition to the relationships for c, we also derive parametric restrictions that must be satisfied for the system to be consistent and for the linear independence to hold. These restrictions are given by the following equation:

$$\nu_j + 2\theta_j + 3\mu_j = 0. \tag{16}$$

This equation is a constraint on the parameters ν_j, θ_j, and μ_j, ensuring that the solutions derived from the application of linear independence remain consistent within the broader context of the system. These parametric restrictions are crucial for maintaining the validity of the solution and ensuring that the derived relationships hold true under the specified conditions.

Provided the following constraints are satisfied, equations (11) and (12) remain unchanged in form:

$$
\begin{cases}
\dfrac{a_1 H}{a_2} = \dfrac{\left(H^4 n_1 + H^2 m_1 + l_1\right)}{H\left(H^4 l_2 + H^2 m_2 + n_2\right)} = \dfrac{H^6 s_1 + H^4 q_1 + H^2 r_1 + p_1}{H\left(H^6 p_2 + H^4 r_2 + H^2 q_2 + s_2\right)} \\[4mm]
= \dfrac{H^8 \Sigma_1 + H^6 \eta_1 + H^4 \sigma_1 + H^2 \gamma_1 + \zeta_1}{H\left(H^8 \zeta_2 + H^6 \gamma_2 + H^4 \sigma_2 + H^2 \eta_2 + \Sigma_2\right)} = \dfrac{(k_1 + \delta_1) H^2 - (\mu_1 + \nu_1) \kappa_1 + e_1}{\left[(e_2 - (\mu_2 + \nu_2) \kappa_1) H^2 + k_2 + \delta_2\right] H} \\[4mm]
= \dfrac{\beta_1 H + \alpha_1 \kappa_1 - \left(\kappa_1^2 + \kappa_2^2\right) H a_1 + \sigma^2 - \omega}{\left(\sigma^2 + \alpha_2 \kappa_1 - \omega\right) H - \left(\kappa_1^2 + \kappa_2^2\right) a_2 + \beta_2}.
\end{cases} \tag{17}
$$

The wave number ω follows directly from equation (17) as:

$$\omega = \frac{1}{H-1}\left[H a_1 \kappa_1^2 + H a_1 \kappa_2^2 + H \sigma^2 + H \alpha_2 \kappa_1 - a_2 \kappa_1^2 - a_2 \kappa_2^2 - H \beta_1 - \sigma^2 - \alpha_1 \kappa_1 + \beta_2\right], \tag{18}$$

where $H - 1 \neq 0$.

A simplified version of equation (11) is considered below to enable its solution:

$$\phi'' + \Delta_1 \phi + \Delta_3 \phi^3 + \Delta_5 \phi^5 + \Delta_7 \phi^7 + \Delta_9 \phi^9 = 0, \tag{19}$$

where

$$\begin{cases} \Delta_1 = \dfrac{\beta_1 H + \alpha_1 \kappa_1 - \left(\kappa_1^2 + \kappa_2^2\right) H a_1 + \sigma^2 - \omega}{\left(\rho_1^2 + \rho_2^2\right) a_1 H}, \\[4mm] \Delta_3 = \dfrac{(k_1 + \delta_1) H^2 - (\mu_1 + \nu_1) \kappa_1 + e_1}{\left(\rho_1^2 + \rho_2^2\right) a_1 H}, \\[4mm] \Delta_5 = \dfrac{H^4 n_1 + H^2 m_1 + l_1}{\left(\rho_1^2 + \rho_2^2\right) a_1 H}, \\[4mm] \Delta_7 = \dfrac{H^6 s_1 + H^4 q_1 + H^2 r_1 + p_1}{\left(\rho_1^2 + \rho_2^2\right) a_1 H}, \\[4mm] \Delta_9 = \dfrac{H^8 \Sigma_1 + H^6 \eta_1 + H^4 \sigma_1 + H^2 \gamma_1 + \zeta_1}{\left(\rho_1^2 + \rho_2^2\right) a_1 H}, \end{cases} \tag{20}$$

provided $\left(\rho_1^2 + \rho_2^2\right) a_1 H \neq 0$.

Balancing ϕ'' and ϕ^9 in equation (19) gives $N = \dfrac{1}{4}$. Letting

$$\phi(\xi) = [U(\xi)]^{\frac{1}{4}}, \tag{21}$$

with $U(\xi) > 0$, transforms equation (19) into the Ordinary Differential Equation (ODE):

$$U''U - \frac{3}{4}U'^2 + 4\Delta_1 U^2 + 4\Delta_5 U^3 + 4\Delta_9 U^4 + 4\Delta_3 U^{\frac{5}{2}} + 4\Delta_7 U^{\frac{7}{2}} = 0. \tag{22}$$

Equation (22) is integrable if

$$\Delta_3 = 0, \ \ \Delta_7 = 0. \tag{23}$$

From (20) and (23), we have constraint conditions:

$$\left.\begin{array}{l} (k_1 + \delta_1) H^2 - (\mu_1 + \nu_1) \kappa_1 + e_1 = 0, \\[2mm] \text{and} \\[2mm] H^6 s_1 + H^4 q_1 + H^2 r_1 + p_1 = 0. \end{array}\right\} \tag{24}$$

Now, equation (22) reduces to

$$4U''U - 3U'^2 + 16\left(\Delta_1 U^2 + \Delta_5 U^3 + \Delta_9 U^4\right) = 0. \tag{25}$$

In the next couple of sections, we will recover the dromions and domain walls of the model.

3. Enhanced direct algebraic approach

We now proceed with applying the integration method in this section. For this purpose, we assume that equation (25) has the following formal solution:

$$U(\xi) = A_0 + \sum_{k=1}^{N} \left[A_k F^k(\xi) + B_k F^{-k}(\xi) \right], \tag{26}$$

where A_0, A_k, and B_k $(k = 1, 2, \ldots, N)$ are constants, with the restriction $A_N^2 + B_N^2 \neq 0$. Additionally, the function $F(\xi)$ adheres to the nonlinear ODE:

$$F'^2(\xi) = \sum_{j=0}^{4} \vartheta_j F^j(\xi), \tag{27}$$

where ϑ_j $(j = 0, 1, 2, 3, 4)$ are constants such that $\vartheta_4 \neq 0$.

For the solution of equation (25), balancing UU'' with U^4 results in $N = 1$. Thus, the form of the solution in equation (26) becomes:

$$U(\xi) = A_0 + A_1 F(\xi) + \frac{B_1}{F(\xi)}, \tag{28}$$

where $A_1^2 + B_1^2 \neq 0$.

By substituting the values from equations (28) and (27) into equation (25), we arrive at

F^4: $16\Delta_9 A_1^4 + 5A_1^2 \vartheta_4 = 0,$

F^3: $64\Delta_9 A_0 A_1^3 + 16\Delta_5 A_1^3 + 8A_1 \vartheta_4 A_0 + 3A_1^2 \vartheta_3 = 0,$

F^2: $96\Delta_9 A_0^2 A_1^2 + 64\Delta_9 A_1^3 B_1 + 48\Delta_5 A_0 A_1^2 + 6A_1 \vartheta_3 A_0 + 16\Delta_1 A_1^2 + A_1^2 \vartheta_2 + 14A_1 \vartheta_4 B_1 = 0,$

F: $64\Delta_9 A_0^3 A_1 + 192\Delta_9 A_0 A_1^2 B_1 + 48\Delta_5 A_0^2 A_1 + 48\Delta_5 A_1^2 B_1 + 32\Delta_1 A_0 A_1 + 4A_1 \vartheta_2 A_0 - A_1^2 \vartheta_1 + 14A_1 \vartheta_3 B_1 = 0,$

F^0: $16\Delta_9 A_0^4 + 192\Delta_9 A_0^2 A_1 B_1 + 96\Delta_9 A_1^2 B_1^2 + 16\Delta_5 A_0^3 + 96\Delta_5 A_0 A_1 B_1 + 16\Delta_1 A_0^2 + 2A_1 \vartheta_1 A_0$

$\qquad + 2B_1 \vartheta_3 A_0 - 3A_1^2 \vartheta_0 + 32\Delta_1 A_1 B_1 + 14A_1 \vartheta_2 B_1 - 3B_1^2 \vartheta_4 = 0,$

F^{-1}: $64\Delta_9 A_0^3 B_1 + 192\Delta_9 A_0 A_1 B_1^2 + 48\Delta_5 A_0^2 B_1 + 48\Delta_5 A_1 B_1^2 + 32\Delta_1 A_0 B_1 + 4B_1 \vartheta_2 A_0 + 14A_1 \vartheta_1 B_1 - B_1^2 \vartheta_3 = 0,$

$$F^{-2}: 96\Delta_9 A_0^2 B_1^2 + 64\Delta_9 A_1 B_1^3 + 48\Delta_5 A_0 B_1^2 + 6B_1 \vartheta_1 A_0 + 14B_1 \vartheta_0 A_1 + 16\Delta_1 B_1^2 + B_1^2 \vartheta_2 = 0,$$

$$F^{-3}: 64\Delta_9 A_0 B_1^3 + 16\Delta_5 B_1^3 + 8B_1 \vartheta_0 A_0 + 3B_1^2 \vartheta_1 = 0,$$

$$F^{-4}: 16\Delta_9 B_1^4 + 5B_1^2 \vartheta_0 = 0.$$

Using Maple to solve the above algebraic equations, we obtain various families of results, which will be presented below:

Family-1: By using $\vartheta_0 = \vartheta_1 = \vartheta_3 = 0$, the result is:

$$A_0 = 0, \quad A_1 = \sqrt{-\frac{5\vartheta_4}{16\Delta_9}}, \quad B_1 = 0, \quad \Delta_1 = -\frac{\vartheta_2}{16}, \quad \Delta_5 = 0, \tag{29}$$

provided $\vartheta_4 \Delta_9 < 0$.

Substituting equation (29) with the established solutions of equation (27) from previous works into equation (28), along with the use of equations (21), (3), and (4), yields the following two types of solutions:

I. Provided $\vartheta_2 > 0$ and $\vartheta_4 < 0$, dromions are formed:

$$q(x, y, t) = \left\{ \sqrt{\frac{5\vartheta_2}{16\Delta_9}} \operatorname{sech}\left[\sqrt{\vartheta_2}\xi\right] \right\}^{\frac{1}{4}} e^{i\left[-\kappa_1 x - \kappa_2 y + (\omega - \sigma^2)t + \sigma W(t)\right]}, \tag{30}$$

$$r(x, y, t) = Hq(x, y, t), \tag{31}$$

where $\Delta_9 > 0$.

II. Provided $\vartheta_2 > 0$ and $\vartheta_4 > 0$, singular waves exist:

$$q(x, y, t) = \left\{ \sqrt{-\frac{5\vartheta_2}{16\Delta_9}} \operatorname{csch}\left[\sqrt{\vartheta_2}\xi\right] \right\}^{\frac{1}{4}} e^{i\left[-\kappa_1 x - \kappa_2 y + (\omega - \sigma^2)t + \sigma W(t)\right]}, \tag{32}$$

$$r(x, y, t) = Hq(x, y, t), \tag{33}$$

where $\Delta_9 < 0$.

Family-2: By using $\vartheta_0 = \frac{\vartheta_2^2}{4\vartheta_4}$, $\vartheta_1 = \vartheta_3 = 0$, $\vartheta_2 < 0$, $\vartheta_4 > 0$, the result is:

$$A_0 = \sqrt{\frac{5\vartheta_2}{32\Delta_9}}, \quad A_1 = \sqrt{-\frac{5\vartheta_4}{16\Delta_9}}, \quad B_1 = 0, \quad \Delta_1 = \frac{\vartheta_2}{8}, \quad \Delta_5 = -\sqrt{\frac{9\vartheta_2\Delta_9}{10}}, \tag{34}$$

provided $\Delta_9 < 0$.

Substituting the well-known solutions of equation (27) from prior reports into equation (34) and using equation (28), along with equations (21), (3), and (4), results in the domain walls:

$$q(x, y, t) = \left\{ \sqrt{\frac{5\vartheta_2}{32\Delta_9}} \left(1 + \tanh\left[\sqrt{-\frac{\vartheta_2}{2}}\xi \right] \right) \right\}^{\frac{1}{4}} e^{i\left[-\kappa_1 x - \kappa_2 y + \left(\omega - \sigma^2 \right) t + \sigma W(t) \right]}, \tag{35}$$

$$r(x, y, t) = Hq(x, y, t), \tag{36}$$

and the singular waves:

$$q(x, y, t) = \left\{ \sqrt{\frac{5\vartheta_2}{32\Delta_9}} \left(1 + \coth\left[\sqrt{-\frac{\vartheta_2}{2}}\xi \right] \right) \right\}^{\frac{1}{4}} e^{i\left[-\kappa_1 x - \kappa_2 y + \left(\omega - \sigma^2 \right) t + \sigma W(t) \right]}, \tag{37}$$

$$r(x, y, t) = Hq(x, y, t). \tag{38}$$

Family-3: Using $\vartheta_1 = \vartheta_3 = 0$, the results is:
Result-1:

$$A_0 = \sqrt{\frac{5\vartheta_2}{32\Delta_9}}, \quad A_1 = \sqrt{-\frac{5\vartheta_2^2}{64\Delta_9\vartheta_0}}, \quad B_1 = 0, \quad \Delta_1 = \frac{\vartheta_2}{8}, \quad \Delta_5 = -\sqrt{\frac{9\vartheta_2\Delta_9}{10}}, \quad \vartheta_4 = \frac{\vartheta_2^2}{4\vartheta_0}, \tag{39}$$

provided $\vartheta_2\Delta_9 > 0$ and $\vartheta_0\Delta_9 < 0$.

Substituting the established solutions of equation (27) into equation (39) and using this in equation (28), along with equations (21), (3), and (4), we obtain two types of Weierstrass Elliptic Function (WEF) solutions as follows:

I. Provided $\vartheta_4 > 0$, the WEF solutions are derived:

$$q(x, y, t) = \left\{ \sqrt{\frac{5\vartheta_2}{32\Delta_9}} + \sqrt{-\frac{5}{16\Delta_9} \left(\frac{3\wp\left[\xi, \frac{\vartheta_2^2}{12} + \vartheta_0\vartheta_4, \frac{\vartheta_2\left(36\vartheta_0\vartheta_4 - \vartheta_2^2 \right)}{216} \right]}{6\wp\left[\xi, \frac{\vartheta_2^2}{12} + \vartheta_0\vartheta_4, \frac{\vartheta_2\left(36\vartheta_0\vartheta_4 - \vartheta_2^2 \right)}{216} \right] + \vartheta_2} \right)} \right\}^{\frac{1}{4}}$$

$$e^{i\left[-\kappa_1 x - \kappa_2 y + \left(\omega - \sigma^2 \right) t + \sigma W(t) \right]}, \tag{40}$$

$$r(x, y, t) = Hq(x, y, t). \tag{41}$$

where $\vartheta_2 < 0$, $\Delta_9 < 0$.

II. When $\vartheta_0 > 0$, the WEF solutions arise:

$$q(x, y, t) = \left\{ \sqrt{\frac{5\vartheta_2}{32\Delta_9}} + \sqrt{-\frac{5\vartheta_2^2}{64\Delta_9}} \left(\frac{6\wp\left[\xi; \frac{\vartheta_2^2}{12} + \vartheta_0\vartheta_4, \frac{\vartheta_2\left(36\vartheta_0\vartheta_4 - \vartheta_2^2\right)}{216}\right] + \vartheta_2}{3\wp'\left[\xi; \frac{\vartheta_2^2}{12} + \vartheta_0\vartheta_4, \frac{\vartheta_2\left(36\vartheta_0\vartheta_4 - \vartheta_2^2\right)}{216}\right]} \right) \right\}^{\frac{1}{4}}$$

$$e^{i\left[-\kappa_1 x - \kappa_2 y + \left(\omega - \sigma^2\right)t + \sigma W(t)\right]}, \tag{42}$$

$$r(x, y, t) = Hq(x, y, t), \tag{43}$$

where $\vartheta_2 < 0$, and $\Delta_9 < 0$.

Result-2:

$$A_0 = \sqrt{\frac{5\vartheta_2}{32\Delta_9}}, \quad A_1 = 0, \quad B_1 = \sqrt{-\frac{5\vartheta_0}{16\Delta_9}}, \quad \Delta_1 = \frac{\vartheta_2}{8}, \quad \Delta_5 = -\sqrt{\frac{9\vartheta_2\Delta_9}{10}}, \quad \vartheta_4 = \frac{\vartheta_2^2}{4\vartheta_0}, \tag{44}$$

provided $\vartheta_2\Delta_9 > 0$, $\vartheta_0\Delta_9 < 0$.

Using the established solutions of equation (27) in equation (44) and substituting them into equation (28), along with equations (21), (3), and (4), we derive two types of WEF solutions:

I. $\vartheta_4 > 0$ implies that the solutions are WEFs:

$$q(x, y, t) = \left\{ \sqrt{\frac{5\vartheta_2}{32\Delta_9}} + \sqrt{-\frac{5\vartheta_2^2}{64\Delta_9}} \left(\frac{3\wp'\left[\xi, \frac{\vartheta_2^2}{12} + \vartheta_0\vartheta_4, \frac{\vartheta_2\left(36\vartheta_0\vartheta_4 - \vartheta_2^2\right)}{216}\right]}{6\wp\left[\xi, \frac{\vartheta_2^2}{12} + \vartheta_0\vartheta_4, \frac{\vartheta_2\left(36\vartheta_0\vartheta_4 - \vartheta_2^2\right)}{216}\right] + \vartheta_2} \right)^{-1} \right\}^{\frac{1}{4}}$$

$$e^{i\left[-\kappa_1 x - \kappa_2 y + \left(\omega - \sigma^2\right)t + \sigma W(t)\right]}, \tag{45}$$

$$r(x, y, t) = Hq(x, y, t), \tag{46}$$

provided $\vartheta_2 < 0$, and $\Delta_9 < 0$.

II. The condition $\vartheta_0 > 0$ implies that the solutions take the form of WEFs:

$$q(x, y, t) = \left\{ \sqrt{\frac{5\vartheta_2}{32\Delta_9}} + \sqrt{-\frac{5}{16\Delta_9}} \left(\frac{6\wp\left[\xi; \dfrac{\vartheta_2^2}{12} + \vartheta_0\vartheta_4, \dfrac{\vartheta_2\left(36\vartheta_0\vartheta_4 - \vartheta_2^2\right)}{216}\right] + \vartheta_2}{3\wp'\left[\xi; \dfrac{\vartheta_2^2}{12} + \vartheta_0\vartheta_4, \dfrac{\vartheta_2\left(36\vartheta_0\vartheta_4 - \vartheta_2^2\right)}{216}\right]} \right)^{-1} \right\}^{\frac{1}{4}}$$

$$e^{i\left[-\kappa_1 x - \kappa_2 y + \left(\omega - \sigma^2\right)t + \sigma W(t)\right]}, \tag{47}$$

$$r(x, y, t) = Hq(x, y, t), \tag{48}$$

provided $\vartheta_2 < 0$, and $\Delta_9 < 0$.

Family-4: Using $\vartheta_0 = \vartheta_1 = 0$, $\vartheta_2 > 0$, the result is:

$$A_0 = 0, \quad A_1 = \sqrt{-\frac{5\vartheta_4}{16\Delta_9}}, \quad B_1 = 0, \quad \Delta_1 = -\frac{\vartheta_2}{16}, \quad \Delta_5 = \sqrt{-\frac{9\Delta_9\vartheta_3^2}{80\vartheta_4}}, \tag{49}$$

provided $\vartheta_4\Delta_9 < 0$.

Using the solutions of equation (27) from earlier reports in equation (49) and substituting them into equation (28), together with equations (21), (3), and (4), we obtain the straddled waves:

$$q(x, y, t) = \left\{ \sqrt{-\frac{5\vartheta_4}{16\Delta_9}} \left(\frac{-\vartheta_2 \operatorname{sech}^2\left[\dfrac{\sqrt{\vartheta_2}\,\xi}{2}\right]}{\pm 2\sqrt{\vartheta_2\vartheta_4}\tanh\left[\dfrac{\sqrt{\vartheta_2}\,\xi}{2}\right] + \vartheta_3} \right) \right\}^{\frac{1}{4}} e^{i\left[-\kappa_1 x - \kappa_2 y + \left(\omega - \sigma^2\right)t + \sigma W(t)\right]}, \tag{50}$$

$$r(x, y, t) = Hq(x, y, t), \tag{51}$$

$$q(x, y, t) = \left\{ \sqrt{-\frac{5\vartheta_4}{16\Delta_9}} \left(\frac{\vartheta_2 \operatorname{csch}^2\left[\dfrac{\sqrt{\vartheta_2}\,\xi}{2}\right]}{\pm 2\sqrt{\vartheta_2\vartheta_4}\coth\left[\dfrac{\sqrt{\vartheta_2}\,\xi}{2}\right] + \vartheta_3} \right) \right\}^{\frac{1}{4}} e^{i\left[-\kappa_1 x - \kappa_2 y + \left(\omega - \sigma^2\right)t + \sigma W(t)\right]}, \tag{52}$$

$$r(x, y, t) = Hq(x, y, t), \tag{53}$$

$$q(x, y, t) = \left\{ \sqrt{-\frac{5\vartheta_4}{16\Delta_9}} \left(\frac{-\vartheta_2\vartheta_3 \operatorname{sech}^2\left[\dfrac{\sqrt{\vartheta_2}\,\xi}{2}\right]}{\vartheta_3^2 - \vartheta_2\vartheta_4\left(1 - \tanh\left[\dfrac{\sqrt{\vartheta_2}\,\xi}{2}\right]\right)^2} \right) \right\}^{\frac{1}{4}} e^{i\left[-\kappa_1 x - \kappa_2 y + \left(\omega - \sigma^2\right)t + \sigma W(t)\right]}, \tag{54}$$

$$r(x, y, t) = Hq(x, y, t),$$ (55)

$$q(x, y, t) = \left\{ \sqrt{-\frac{5\vartheta_4}{16\Delta_9} \left(\frac{\vartheta_2 \vartheta_3 \operatorname{csch}^2 \left[\frac{\sqrt{\vartheta_2}\,\xi}{2} \right]}{\vartheta_3^2 - \vartheta_2 \vartheta_4 \left(1 - \coth \left[\frac{\sqrt{\vartheta_2}\,\xi}{2} \right] \right)^2} \right)} \right\}^{\frac{1}{4}} e^{i\left[-\kappa_1 x - \kappa_2 y + (\omega - \sigma^2) t + \sigma W(t) \right]},$$ (56)

$$r(x, y, t) = Hq(x, y, t),$$ (57)

provided $\vartheta_4 > 0$ and $\Delta_9 < 0$.

4. Addendum to Kudryashov's approach

Following the integration method, we assume the formal solution of equation (25) takes the form below:

$$U(\xi) = \sum_{i=0}^{M} \tau_i P^i(\xi).$$ (58)

With τ_i $(i = 0, 1, 2, \ldots, M)$ denoting constants such that $\tau_M \neq 0$, the function $P(\xi)$ satisfies the ODE below:

$$P'^2(\xi) = P^2(\xi) \left[1 - \varkappa P^{2s}(\xi) \right] \ln^2 K, \ 0 < K \neq 1.$$ (59)

Given that $\varkappa \neq 0$ and s is an integer, a balance between UU'' and U^4 in equation (25) gives $2M + 2s = 4M$, leading to the conclusion $M = s$.

Case-I: Assigning $s = 1$, the expression for the formal solution given in (58) simplifies to:

$$U(\xi) = \tau_0 + \tau_1 P(\xi), \ \tau_1 \neq 0,$$ (60)

where

$$P'^2(\xi) = P^2(\xi) \left[1 - \varkappa P^2(\xi) \right] \ln^2 K.$$ (61)

The substitution of equations (60) and (61) into equation (25) yields:

$$P^4: \ -5\varkappa \tau_1^2 \ln^2 K + 16\Delta_9 \tau_1^4 = 0,$$

$$P^3: \ -8\varkappa \tau_0 \tau_1 \ln^2 K + 64\Delta_9 \tau_0 \tau_1^3 + 16\Delta_5 \tau_1^3 = 0,$$

$$P^2: 96\Delta_9 \tau_0^2 \tau_1^2 + \tau_1^2 \ln^2 K + 48\Delta_5 \tau_0 \tau_1^2 + 16\Delta_1 \tau_1^2 = 0,$$

$$P: 64\Delta_9 \tau_0^3 \tau_1 + 4\tau_0 \tau_1 \ln^2 K + 48\Delta_5 \tau_0^2 \tau_1 + 32\Delta_1 \tau_0 \tau_1 = 0,$$

$$P^0: 16\Delta_9 \tau_0^4 + 16\Delta_5 \tau_0^3 + 16\Delta_1 \tau_0^2 = 0.$$

By employing Maple to solve the aforementioned system, we obtain the following result:

$$\tau_0 = 0, \quad \tau_1 = \sqrt{\frac{5\varkappa \ln^2 K}{16\Delta_9}}, \quad \Delta_1 = -\frac{\ln^2 K}{16}, \quad \Delta_5 = 0, \tag{62}$$

provided $\varkappa\Delta_9 > 0$.

The exact solutions can be obtained by combining equation (62) with the known results of equation (61) and substituting the result into equation (26):

$$q(x, y, t) = \left\{ \sqrt{\frac{5\varkappa \ln^2 K}{16\Delta_9}} \left(\frac{4C}{4C^2 K^\xi + \varkappa K^{-\xi}} \right) \right\}^{\frac{1}{4}} e^{i\left[-\kappa_1 x - \kappa_2 y + \left(\omega - \sigma^2\right)t + \sigma W(t)\right]}, \tag{63}$$

$$r(x, y, t) = Hq(x, y, t), \tag{64}$$

where C is a constant. Expressions (63) and (64) describe exact solutions that take the form of solitary waves:

$$q(x, y, t) = \left\{ \sqrt{\frac{5\varkappa \ln^2 K}{16\Delta_9}} \left(\frac{4C}{(4C^2 + \varkappa)\cosh[\xi \ln K] + (4C^2 - \varkappa)\sinh[\xi \ln K]} \right) \right\}^{\frac{1}{4}} e^{i\left[-\kappa_1 x - \kappa_2 y + \left(\omega - \sigma^2\right)t + \sigma W(t)\right]}, \tag{65}$$

$$r(x, y, t) = Hq(x, y, t), \tag{66}$$

Specifically, if $\varkappa = 4C^2$, solutions (65) and (66) can be expressed as dromions:

$$q(x, y, t) = \left\{ \sqrt{\frac{5 \ln^2 K}{16\Delta_9}} \operatorname{sech}[\xi \ln K] \right\}^{\frac{1}{4}} e^{i\left[-\kappa_1 x - \kappa_2 y + \left(\omega - \sigma^2\right)t + \sigma W(t)\right]}, \tag{67}$$

$$r(x, y, t) = Hq(x, y, t), \tag{68}$$

provided $\Delta_9 > 0$.

When $\varkappa = -4C^2$, the solutions (65) and (66) transform into singular waves:

$$q(x, y, t) = \left\{ \sqrt{-\frac{5\ln^2 K}{16\Delta_9}} \operatorname{csch}\left[\xi \ln K\right] \right\}^{\frac{1}{4}} e^{i\left[-\kappa_1 x - \kappa_2 y + \left(\omega - \sigma^2\right)t + \sigma W(t)\right]}, \tag{69}$$

$$r(x, y, t) = Hq(x, y, t), \tag{70}$$

provided $\Delta_9 < 0$.

Case-II: If $s = 2$, equation (25) takes the form:

$$U(\xi) = \tau_0 + \tau_1 P(\xi) + \tau_2 P^2(\xi), \quad \tau_2 \neq 0, \tag{71}$$

where

$$P'^2(\xi) = P^2(\xi)\left[1 - \varkappa P^4(\xi)\right]\ln^2 K. \tag{72}$$

Inserting equations (71) and (72) within equation (25) leads to:

P^8: $-20\varkappa\tau_2^2\ln^2 K + 16\Delta_9\tau_2^4 = 0,$

P^7: $-32\varkappa\tau_1\tau_2\ln^2 K + 64\Delta_9\tau_1\tau_2^3 = 0,$

P^6: $-32\varkappa\tau_0\tau_2\ln^2 K - 9\varkappa\tau_1^2\ln(K)^2 + 64\Delta_9\tau_0\tau_2^3 + 96\Delta_9\tau_1^2\tau_2^2 + 16\Delta_5\tau_2^3 = 0,$

P^5: $-12\varkappa\tau_0\tau_1\ln^2 K + 192\Delta_9\tau_0\tau_1\tau_2^2 + 64\Delta_9\tau_1^3\tau_2 + 48\Delta_5\tau_1\tau_2^2 = 0,$

P^4: $96\Delta_9\tau_0^2\tau_2^2 + 192\Delta_9\tau_0\tau_1^2\tau_2 + 16\Delta_9\tau_1^4 + 4\tau_2^2\ln^2 K + 48\Delta_5\tau_0\tau_2^2 + 48\Delta_5\tau_1^2\tau_2 + 16\Delta_1\tau_2^2 = 0,$

P^3: $192\Delta_9\tau_0^2\tau_1\tau_2 + 64\Delta_9\tau_0\tau_1^3 + 8\tau_1\tau_2\ln^2 K + 96\Delta_5\tau_0\tau_1\tau_2 + 16\Delta_5\tau_1^3 + 32\Delta_1\tau_1\tau_2 = 0,$

P^2: $64\Delta_9\tau_0^3\tau_2 + 96\Delta_9\tau_0^2\tau_1^2 + 16\tau_0\tau_2\ln^2 K + \tau_1^2\ln^2 K + 48\Delta_5\tau_0^2\tau_2 + 48\Delta_5\tau_0\tau_1^2 + 32\Delta_1\tau_0\tau_2 + 16\Delta_1\tau_1^2 = 0,$

P: $64\Delta_9\tau_0^3\tau_1 + 4\tau_0\tau_1\ln^2 K + 48\Delta_5\tau_0^2\tau_1 + 32\Delta_1\tau_0\tau_1 = 0,$

P^0: $16\Delta_9\tau_0^4 + 16\Delta_5\tau_0^3 + 16\Delta_1\tau_0^2 = 0.$

Using Maple to solve the algebraic system above, we arrive at:

$$\tau_0 = 0, \quad \tau_1 = 0, \quad \tau_2 = \sqrt{\frac{5\varkappa \ln^2 K}{4\Delta_9}}, \quad \Delta_1 = -\frac{\ln^2 K}{4}, \quad \Delta_5 = 0, \tag{73}$$

provided $\varkappa \Delta_9 > 0$.

Incorporating (73) with the established solutions of equation (72) derived from into (71) yields the explicit solutions:

$$q(x, y, t) = \left\{ \sqrt{\frac{5\varkappa \ln^2 K}{4\Delta_9}} \left(\frac{4C}{4C^2 K^{2\xi} + \varkappa K^{-2\xi}} \right) \right\}^{\frac{1}{4}} e^{i\left[-\kappa_1 x - \kappa_2 y + \left(\omega - \sigma^2 \right) t + \sigma W(t) \right]}, \tag{74}$$

$$r(x, y, t) = Hq(x, y, t). \tag{75}$$

The forms given in (74) and (75) can be identified as straddled wave structures:

$$q(x, y, t) = \left\{ \sqrt{\frac{5\varkappa \ln^2 K}{4\Delta_9}} \left(\frac{4C}{(4C^2 + \varkappa) \cosh\left[2\xi \ln K\right] + (4C^2 - \varkappa) \sinh\left[2\xi \ln K\right]} \right) \right\}^{\frac{1}{4}} e^{i\left[-\kappa_1 x - \kappa_2 y + \left(\omega - \sigma^2 \right) t + \sigma W(t) \right]}, \tag{76}$$

$$r(x, y, t) = Hq(x, y, t), \tag{77}$$

Specifically, if $\varkappa = 4C^2$, solutions (76) and (77) can be expressed as dromions.

$$q(x, y, t) = \left\{ \sqrt{\frac{5 \ln^2 K}{4\Delta_9}} \operatorname{sech}\left[2\xi \ln K\right] \right\}^{\frac{1}{4}} e^{i\left[-\kappa_1 x - \kappa_2 y + \left(\omega - \sigma^2 \right) t + \sigma W(t) \right]}, \tag{78}$$

$$r(x, y, t) = Hq(x, y, t), \tag{79}$$

provided $\Delta_9 > 0$.

When $\varkappa = -4C^2$ transforms the solutions (76) and (77) into singular waves.

$$q(x, y, t) = \left\{ \sqrt{-\frac{5 \ln^2 K}{4\Delta_9}} \operatorname{csch}\left[2\xi \ln K\right] \right\}^{\frac{1}{4}} e^{i\left[-\kappa_1 x - \kappa_2 y + \left(\omega - \sigma^2 \right) t + \sigma W(t) \right]}, \tag{80}$$

$$r(x, y, t) = Hq(x, y, t), \tag{81}$$

provided $\Delta_9 < 0$.

Similarly, selecting different values for the parameter s yields further solutions to the system (1) and (2); however, some of these have been excluded from the current discussion for readability.

5. Results and discussion

Both schemes offer several advantages. They enable closed-form retrieval, providing explicit analytical formulas rather than merely numerical profiles, which allows direct inspection of localization lengths, amplitudes, and phases. Their parameter transparency reveals how higher-order Self-Phase Modulation (SPM) coefficients, Bragg reflectivity parameters, and noise intensity influence the resulting solution manifolds and existence domains. Moreover, the complementarity and verification between the polynomial and rational ansätze ensures that independently derived expressions converge to the same families of solutions, serving as mutual validation. Finally, the approaches exhibit continuity to limiting cases, reducing smoothly to deterministic or lower-order nonlinear regimes, thereby situating the newly retrieved solutions within the broader landscape of known models.

The approaches are ansatz-based and best suited to balanceable polynomial/rational structures and separable or traveling-wave reductions; hence they may not capture non-ansatz solution branches. They do not, by themselves, provide spectral stability theory or full stochastic statistics (e.g., probability of rare transitions), and are not a substitute for numerical continuation or stochastic simulation when exploring global bifurcations or noise-induced switching. Nonetheless, for the present strongly nonlinear Bragg-grating model, they deliver closed-form families and explicit parameter dependencies that are otherwise difficult to obtain.

Both the enhanced direct algebraic route and the Kudryashov addendum yield coincident families of gap dromions and domain walls with identical existence constraints, thereby cross-validating the closed-form expressions reported below.

Figures 1 and 2 provide a comprehensive visualization of the dromions and domain walls $q(x, y, t)$ and $r(x, y, t)$, described by the complex-valued solutions (30)-(31) and (35)-(36), respectively, focusing on their structural characteristics under the influence of key physical parameters: $H = 1.5$, $\vartheta_2 = 1$, $\kappa_1 = 1$, $\kappa_2 = 1$, $a_1 = 1$, $a_2 = 1$, $\alpha_1 = 1$, $\alpha_2 = 1$, $\beta_1 = 1$, $\beta_2 = 1$, $\rho_1 = 1$, $\rho_2 = 1$, $c = 1$, $\Sigma_1 = 1$, $\eta_1 = 1$, $\sigma_1 = 1$, $\gamma_1 = 1$, and $\zeta_1 = 1$. These figures examine the evolution and structure of these dromions and domain walls through detailed surface plots of their real and imaginary components while systematically investigating the influence of multiplicative white noise, parameterized by $\sigma = 0, 2, 3$, and 4. Each figure consists of sixteen subfigures, labeled (Figure 1a-1p), and collectively portrays the spatiotemporal dynamics of both dromions and domain walls types under increasing stochastic perturbations.

In all panels, $r = Hq$ with $H = 1.5$; thus, r has the same profile as q, scaled in amplitude by 1.5. The multiplicative noise σ enters only through the common phase factor in Eqs. (30)-(31) and (35)-(36), leaving the dromion envelope $|q|$ (and $|r|$) invariant with σ. Differences across σ affect only the phase, not the localization or peak modulus.

Figure 1 presents a detailed investigation of the dromions $q(x, y, t)$ and $r(x, y, t)$, which are governed by the complex-valued forms in equations (30) and (31). This figure comprises sixteen subfigures, labeled 1a-1p, that provide surface plots illustrating the real and imaginary parts of these dromions under the influence of multiplicative white noise at different intensities: $\sigma = 0$, $\sigma = 2$, $\sigma = 3$, and $\sigma = 4$. Specifically, Figures 1a-1d correspond to the case of $\sigma = 0$, where both the real and imaginary parts of the solutions display clean, sharply localized peaks characteristic of dromions. The dromion structure is highly coherent and symmetric, with the energy concentrated in a confined spatial region, demonstrating the classic behavior of dromions in a noise-free medium.

As the noise intensity increases to $\sigma = 2$ (Figures 1e-1h), small perturbations begin to emerge on the dromion profiles. Although the core dromion structure is preserved, a slight broadening of the dromion and minor irregularities in amplitude distribution can be observed, reflecting the onset of stochastic influence. At $\sigma = 3$, depicted in Figures 1i-1l, the dromion undergoes more noticeable deformation. The amplitude becomes slightly attenuated, and the spatial confinement loosens, indicating the destabilizing impact of moderate noise levels. Figures 1m-1p, corresponding to $\sigma = 4$, show that the dromion profile is further degraded: the amplitude diminishes significantly, and the dromion spreads over a broader spatial domain, accompanied by pronounced asymmetry. These findings highlight that the dromions $q(x, y, t)$ and $r(x, y, t)$ remain

relatively stable under weak noise but become increasingly susceptible to dispersion and amplitude reduction as the noise level rises. Nonetheless, even at high noise levels, the dromion structure does not entirely vanish, illustrating a degree of robustness in the presence of stochastic perturbations.
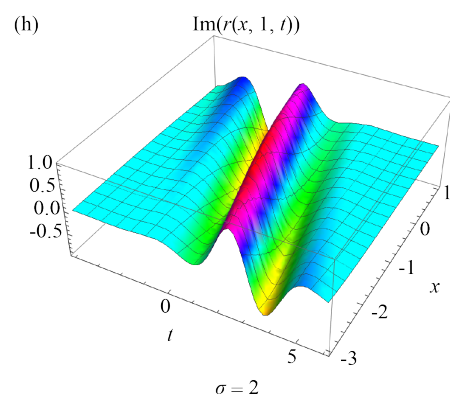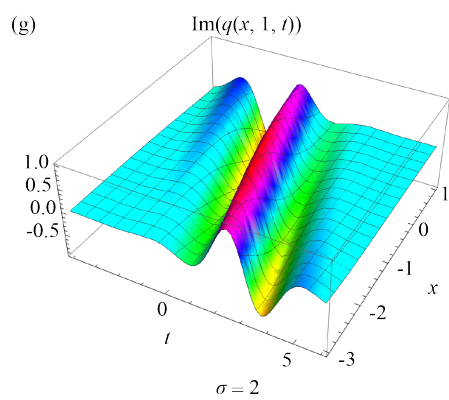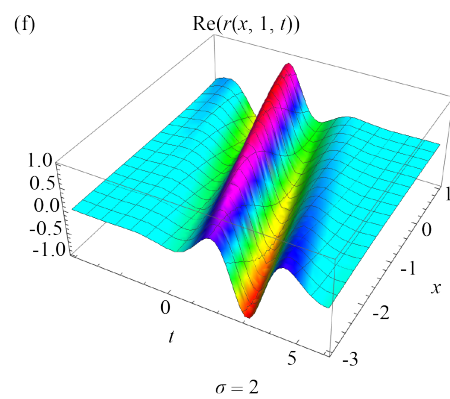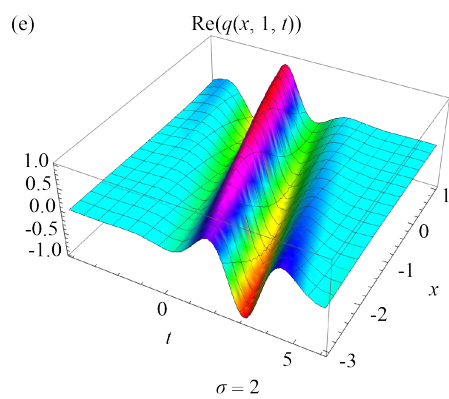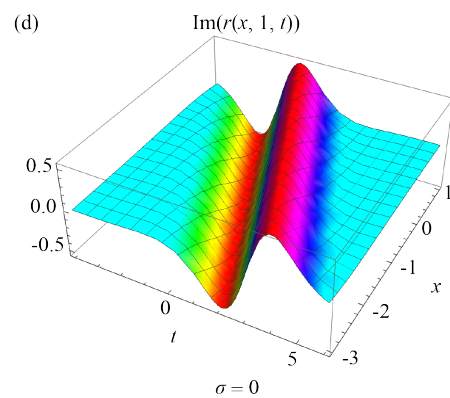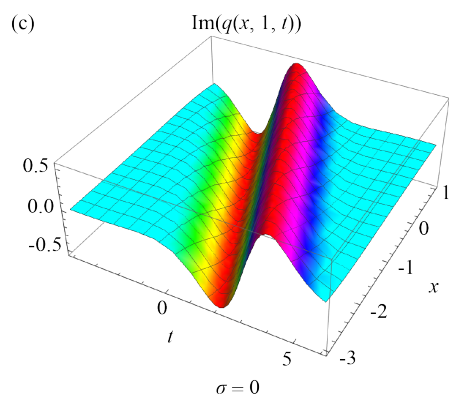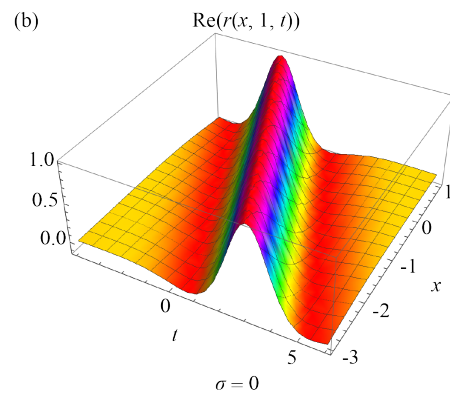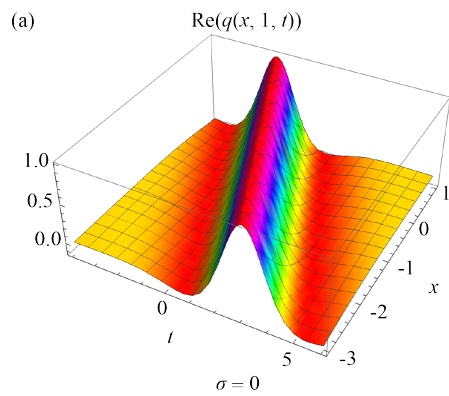
Figure 2 explores the behavior of domain walls $q(x, y, t)$ and $r(x, y, t)$, derived from the complex-valued solutions (35) and (36). Like Figure 1, it contains sixteen subfigures (2a-2p) that provide surface plots for the real and imaginary components of the domain walls under varying strengths of multiplicative white noise. Figures 2a-2d illustrate the case of $\sigma = 0$, where the domain walls exhibit their defining characteristic—a localized intensity dip on a continuous background. The real and imaginary parts both show a smooth and symmetric trough at the domain wall center, surrounded by a flat, unperturbed field, capturing the essential profile of noise-free domain walls.

With the introduction of noise at $\sigma = 2$ (Figures 2e-2h), the domain wall retains its dip structure, but slight oscillations appear around the background, indicating initial disturbances. The domain wall core remains distinct, though the surrounding field begins to exhibit signs of stochastic fluctuations. At $\sigma = 3$, as seen in Figures 2i-2l, the trough becomes shallower and the background becomes increasingly irregular, suggesting that the domain wall is less resilient to noise compared to its behavior at lower levels. The domain wall dip is still discernible but starts losing its symmetry and sharpness. Under the strongest noise condition $\sigma = 4$ (Figures 2m-2p), the domain wall is considerably distorted: the depth of the trough is reduced, the surrounding background is heavily modulated, and the overall coherence of the domain wall structure deteriorates. However, remnants of the domain wall dip persist, indicating that despite the high-intensity noise, the domain wall maintains a recognizable, albeit weakened, profile.

Collectively, Figures 1 and 2 offer a comparative analysis of dromion and domain wall behavior in the presence of multiplicative white noise. Dromions, represented by localized peaks, are more visibly impacted by noise in terms of amplitude suppression and spatial spreading. Domain walls, characterized by localized intensity dips, demonstrate relatively better resilience in terms of maintaining their core structure but suffer from background instability and reduced contrast under noise. Both dromions and domain walls $q(x, y, t)$ and $r(x, y, t)$ show consistent behaviors across corresponding subfigures, reinforcing the validity of the underlying mathematical models and confirming the influence of stochastic perturbations on nonlinear dynamics. These results contribute valuable insight into the stability properties of dromions and domain walls in noisy environments, a critical factor in designing robust nonlinear optical systems.

In Bragg-grating media, the periodic refractive index produces a spectral bandgap that prevents the propagation of linear waves. Localized gap structures appear when dispersive reflectivity is balanced by Self-Phase Modulation (SPM). The gap dromions presented here are $(2+1)D$ solitary entities that are exponentially localized in both transverse coordinates (x, y) and evolve along the propagation direction. Physically, they represent self-trapped packets whose carrier frequency lies within the bandgap, with energy circulation sustained by the grating reflectivity. The domain walls are heteroclinic fronts connecting two distinct uniform states, such as backgrounds with different phase or amplitude allowed by the nonlinear dispersion. These can be interpreted as optical switching interfaces in a grating-based medium. High-order SPM terms (cubic, quintic, septic, and nonic) account for strong-field corrections beyond the Kerr regime. These terms modify the effective nonlinearity, which in turn influences the amplitude, width, and phase structure. Multiplicative white noise represents rapid fluctuations of material or grating parameters. Parametrically, it alters the coefficients appearing in the closed-form solutions, producing predictable variations in localization and phase while preserving the algebraic balance that defines the exact profiles.

In the present parametrized setting, multiplicative noise enters through the solution coefficients and modulates the power P, the localization lengths (L_x, L_y), and the phase shift $\Delta\phi$ in a controlled way. Increasing the noise intensity reduces coherence, resulting in wider (L_x, L_y) and smaller peak amplitude, and it can also bias the phase offset of domain walls. The gap-localization mechanism itself remains intact within the derived existence conditions.
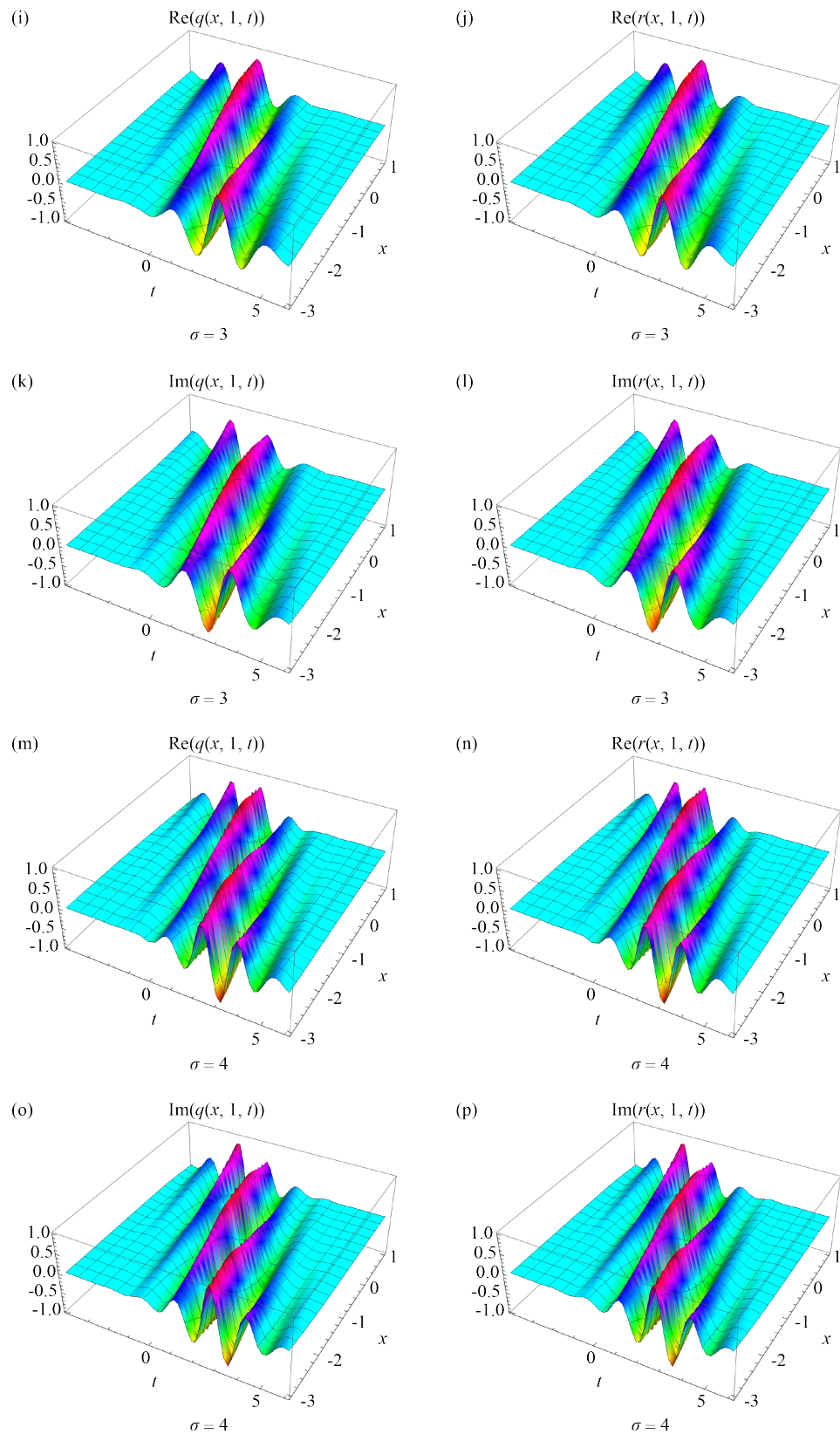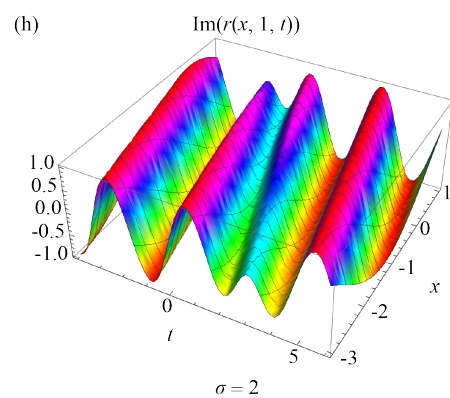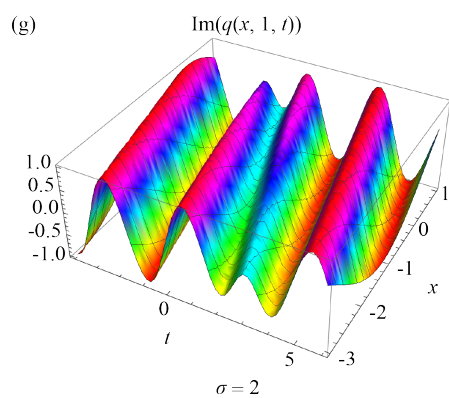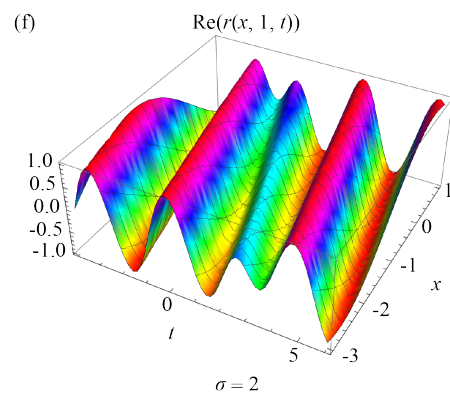
(i) Re($q(x, 1, t)$)

(j) Re($r(x, 1, t)$)

$\sigma = 3$

$\sigma = 3$

(k) Im($q(x, 1, t)$)

(l) Im($r(x, 1, t)$)

$\sigma = 3$

$\sigma = 3$

(m) Re($q(x, 1, t)$)

(n) Re($r(x, 1, t)$)

$\sigma = 4$

$\sigma = 4$
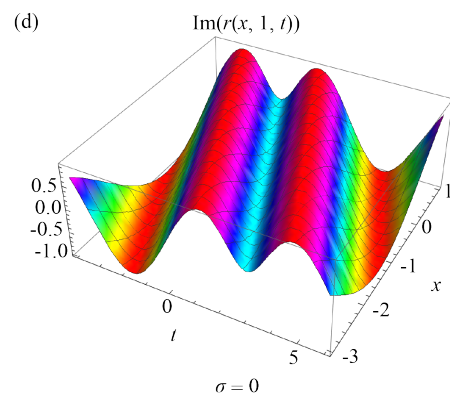
(o) Im($q(x, 1, t)$)

(p) Im($r(x, 1, t)$)

$\sigma = 4$

$\sigma = 4$

Figure 1. Profile of dromions (30) and (31)

(i) Re(q(x, 1, t)), σ = 3

(j) Re(r(x, 1, t)), σ = 3

(k) Im(q(x, 1, t)), σ = 3

(l) Im(r(x, 1, t)), σ = 3

(m) Re(q(x, 1, t)), σ = 4

(n) Re(r(x, 1, t)), σ = 4

(o) Im(q(x, 1, t)), σ = 4

(p) Im(r(x, 1, t)), σ = 4
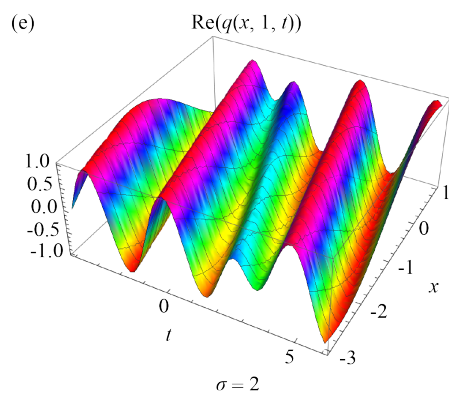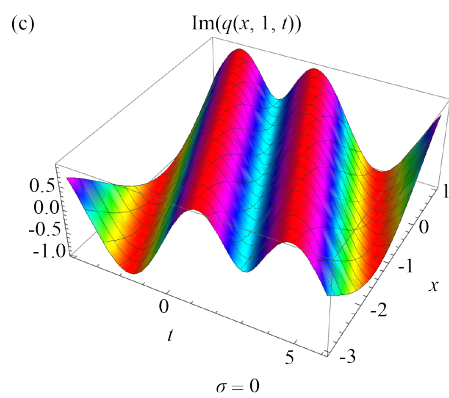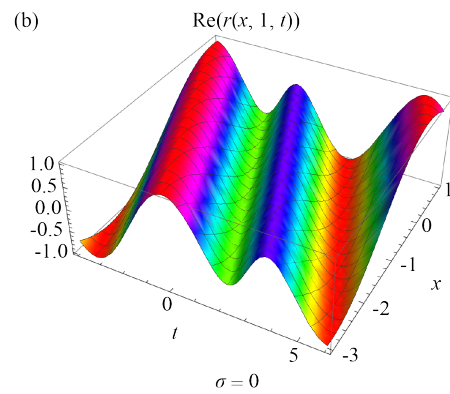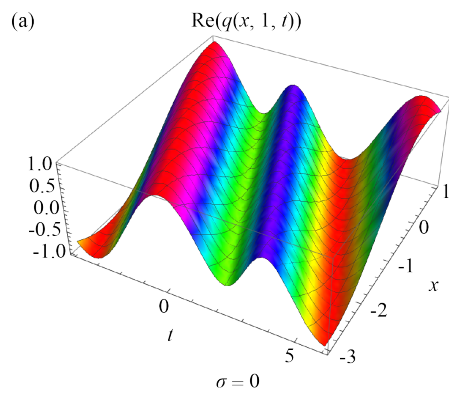
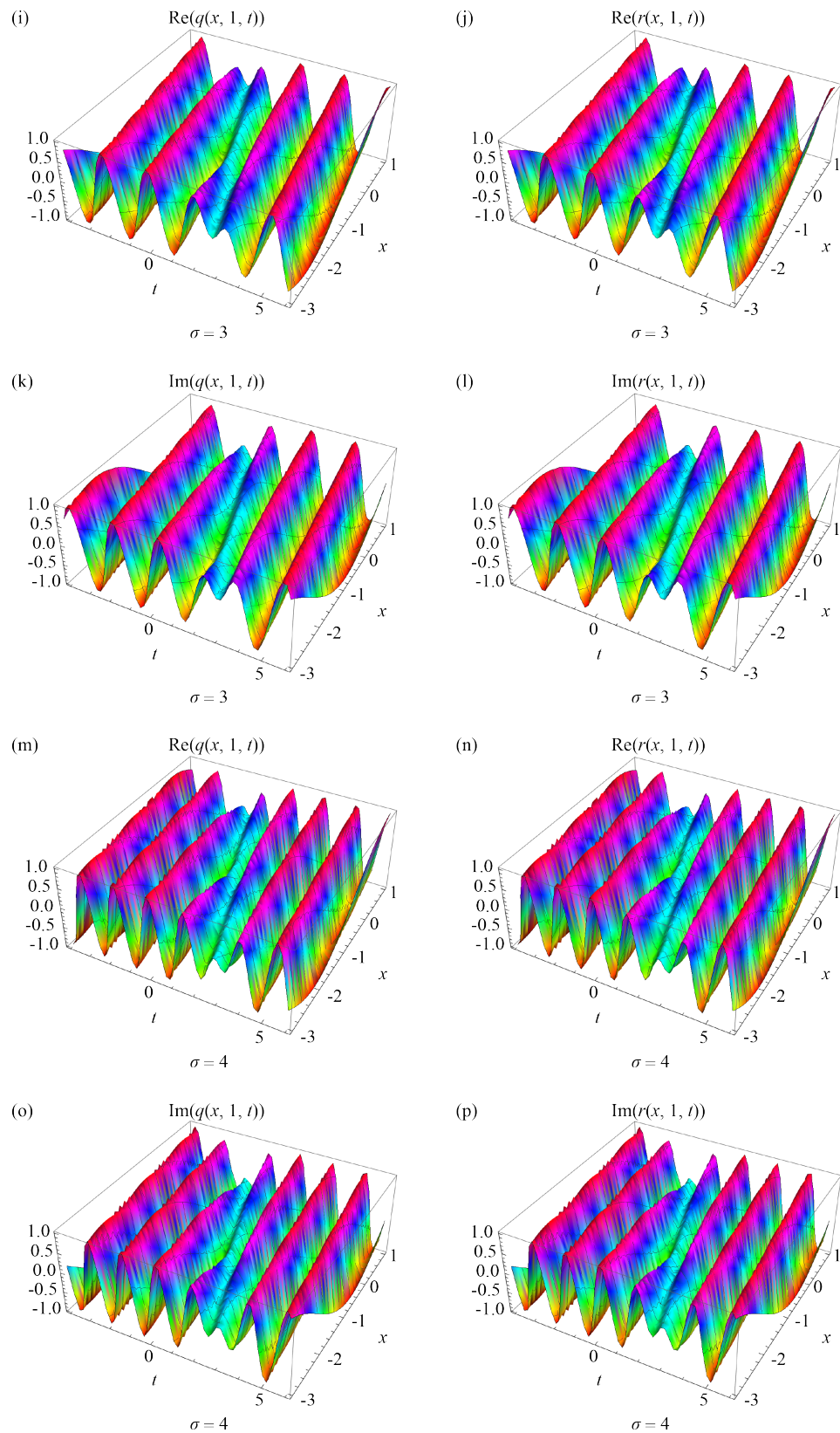**Figure 2.** Profile of domain walls (35) and (36)

The reported gap dromions and domain walls can be observed experimentally in Bragg-grating platforms such as optical fibers, planar gratings, and grating-coupled waveguide arrays. Dromions correspond to $(2+1)D$ self-trapped packets whose carrier lies in the bandgap and can be detected as localized bright spots in near-field intensity maps at the output facet, or as sharp defect-like features in transmission or reflection spectra at a detuning Δ inside the gap. Domain walls act as optical switching interfaces between two admissible background states and may be detected through a measurable phase step $\Delta\phi$ across the interface using interferometry, or through bistable switching traces in input-output characteristics. In the chosen parametrization, high-order SPM coefficients tune amplitude, width, and phase structure, while multiplicative noise introduces parametric broadening that widens the localization lengths (L_x, L_y), lowers the peak amplitude, and induces mild phase jitter. These effects can be quantified using the power P, widths, detuning Δ, and phase shift $\Delta\phi$ derived below.

We employ a Nonlinear Auxiliary-Equation (NAE) approach in combination with the enhanced direct algebraic method and the Kudryashov addendum, since the present Bragg-grating model admits reductions with a balanceable polynomial structure. In such cases, representing the solution through an auxiliary function that satisfies a low-order ordinary differential equation, such as Riccati, logistic, or elliptic type, preserves closure under differentiation and nonlinearity. This yields closed-form solution families with explicit parameter constraints that include high-order SPM coefficients, coupling or reflectivity parameters, and noise intensity.

All exact profiles obtained in this work result from reductions that preserve polynomial balance between dispersive reflectivity and cubic-quintic-septic-nonic SPM. Multiplicative noise is incorporated parametrically through coefficients that appear in the closed-form expressions. We do not claim universality of the NAE method beyond this class. Stability analysis and statistical properties lie outside the present scope and are identified as directions for future investigation.

Beyond the enhanced direct algebraic approach and the Kudryashov addendum used here, a wide range of symbolic ansatz methods exist for nonlinear partial differential equations, including the exp-function framework, the (G'/G)-expansion and its improved variants, extended tanh or coth and sine-cosine schemes, Jacobi-elliptic and F-expansions, as well as projective Riccati and first-integral constructions (see, for example [30–34]). These methods are suitable when the reduced ordinary differential equation admits a finite algebraic balance between dispersive and polynomial or rational nonlinearities. In the current Bragg-grating context, dispersive reflectivity together with the cubic-quintic-septic-nonic SPM structure generates exactly such balanceable polynomial forms. Moreover, multiplicative white noise enters parametrically in a manner that preserves algebraic closure. For this reason, the enhanced direct algebraic approach provides explicit polynomial ansätze with transparent balance conditions, while the Kudryashov addendum contributes complementary rational forms. Together they yield closed-form gap-dromion and domain-wall families with explicit parameter dependencies. Alternative symbolic schemes may produce functionally equivalent solutions under suitable transformations, although they often require additional matching conditions, such as elliptic-modulus selections or auxiliary mappings, which can obscure the explicit dependence on high-order SPM and noise coefficients that is central to the present classification.

While several symbolic frameworks cited in [30–34] could be adapted to the reduced equations, the pair employed here most effectively preserves algebraic balance and maintains explicit dependence on the high-order SPM and multiplicative-noise coefficients, which is essential for the classification presented in this work.

In addition to symbolic and ansatz-based frameworks, non-symbolic techniques such as the direct mapping method and the variational or collective-coordinate approach have proven successful in many nonlinear wave models. These methods are often simpler and require less algebraic manipulation [35–37]. The direct mapping approach constructs a transformation that relates the target equation or its reduction to a base equation with known solutions, from which the profiles can be obtained by inversion. Its efficiency depends on finding a suitable, preferably invertible, mapping that respects the model's coefficients and coupling parameters. Variational methods, by contrast, assume a trial function and derive evolution equations for a small set of collective parameters from an effective Lagrangian, yielding low-dimensional dynamics for quantities such as amplitude, width, and phase. In the present Bragg-grating problem, characterized by dispersive reflectivity, high-order self-phase modulation, and parametric multiplicative noise, symbolic approaches are preferred because they produce closed-form gap-dromion and domain-wall families with explicit dependence on nonlinear and noise coefficients, which is fundamental to our classification. Nevertheless, non-symbolic methods

remain complementary: mapping techniques may generate alternative formulations, and variational tools are suitable for perturbative robustness and slow-modulation studies. These directions represent promising extensions for future work.

All obtained profiles were verified by direct substitution and residual analysis, confirming that they satisfy the reduced equations exactly within computational accuracy.

6. Conclusions

This paper successfully recovers gap dromion solutions governed by a SPM structure characterized by a cubic-quintic-septic-nonic nonlinearity, under the influence of multiplicative white noise. To achieve this, two distinct integration approaches were employed, both of which led to the derivation of exact analytical solutions. These solutions have been systematically listed and categorized according to their functional forms and physical behavior.

Among the obtained results, a notable class of solutions expressed in terms of Weierstrass' elliptic functions was identified. These elliptic function solutions, under particular parameter constraints, can be reduced to dromion-type solutions. While the specific parameter values leading to such reductions are not explicitly provided in the current study, this omission is deliberate due to their straightforward derivation and redundancy in the context of the main results.

The outcomes presented in this work hold significant potential in the field of fiber optic technology, particularly in addressing the issue of low CD by introducing dispersive reflectivity through nonlinear wave structures such as gap dromions and domain walls. The two analytical schemes employed here proved effective in capturing not only the solution forms but also the associated parameter conditions necessary for the existence of such localized structures.

Encouraged by the current findings, future research will extend this framework by incorporating additional analytical and numerical integration schemes. These include, but are not limited to, the improved Adomian Decomposition Method and the Laplace-Adomian Decomposition Method, both of which have shown considerable promise in handling nonlinear systems of this type.

The results derived from ongoing and future studies will be disseminated progressively through several journal publications, aiming to broaden the impact and applicability of this research within the optical soliton and nonlinear wave communities.

Conflict of interest

The authors declare no competing financial interest.

References

[1] Murad MAS, Arnous AH, Faridi WA, Iqbal M, Nisar KS, Kumar S. Two distinct algorithms for conformable time-fractional nonlinear Schrödinger equations with Kudryashov's generalized non-local nonlinearity and arbitrary refractive index. *Optical and Quantum Electronics*. 2024; 56: 1320. Available from: https://doi.org/10.1007/s11082-024-07223-8.

[2] Zhou Q, Liu L, Liu Y, Yu H, Yao P, Wei C, et al. Exact optical solitons in metamaterials with cubic-quintic nonlinearity and third-order dispersion. *Nonlinear Dynamics*. 2015; 80: 1365-1371. Available from: https://doi.org/10.1007/s11071-015-1948-x.

[3] Murad MAS. Optical solutions for perturbed conformable Fokas-Lenells equation via Kudryashov auxiliary equation method. *Modern Physics Letters B*. 2024; 39(7): 2450418. Available from: https://doi.org/10.1142/S0217984924504189.

[4] Ullah N, Rehman HU, Imran MA, Abdeljawad T. Highly dispersive optical solitons with cubic law and cubic-quintic-septic law nonlinearities. *Results in Physics*. 2020; 17: 103021. Available from: https://doi.org/10.1016/j.rinp.2020.103021.

[5] Mirzazadeh M, Sharif A, Hashemi MS, Akgül A, Din SME. Optical solitons with an extended (3 + 1)-dimensional nonlinear conformable Schrödinger equation including cubic-quintic nonlinearity. *Results in Physics*. 2023; 49(8): 106521. Available from: https://doi.org/10.1016/j.rinp.2023.106521.

[6] Kumar V, Jiwari R, Djurayevich AR, Khudoyberganov MU. Hyperbolic (3 + 1)-dimensional nonlinear Schrödinger equation: Lie symmetry analysis and modulation instability. *Journal of Mathematics*. 2022; 2022: 1-8. Available from: https://doi.org/10.1155/2022/9050272.

[7] Wang G. A new (3 + 1)-dimensional Schrödinger equation: derivation, soliton solutions and conservation laws. *Nonlinear Dynamics*. 2021; 104: 1595-1602. Available from: https://doi.org/10.1007/s11071-021-06359-6.

[8] Younas U, Seadawy AR, Younis M, Rizvi STR. Optical solitons and closed form solutions to the (3 + 1)-dimensional resonant nonlinear Schrödinger dynamical wave equation. *International Journal of Modern Physics B*. 2020; 34(30): 2050291. Available from: https://doi.org/10.1142/S0217979220502914.

[9] Murad MAS. Analyzing the time-fractional (3 + 1)-dimensional nonlinear Schrödinger equation: A new Kudryashov approach and optical solutions. *International Journal of Computer Mathematics*. 2024; 101: 524-537. Available from: https://doi.org/10.1080/00207160.2024.2351110.

[10] Tang L. Bifurcations and optical solitons for the coupled nonlinear Schrödinger equation in optical fiber Bragg gratings. *Journal of Optics*. 2023; 52: 1388-1398. Available from: https://doi.org/10.1007/s12596-022-00963-4.

[11] Shahzad T, Baber MZ, Sulaiman TA, Ahmad MO, Yasin MW. Optical wave profiles for the higher order cubic-quartic Bragg-gratings with anti-cubic nonlinear form. *Optical and Quantum Electronics*. 2024; 56: 67. Available from: https://doi.org/10.1007/s11082-023-05615-w.

[12] Rehman S, Bilal M, Ahmad J. Highly dispersive optical and other soliton solutions to fiber Bragg gratings with the application of different mechanisms. *International Journal of Modern Physics B*. 2022; 36: 2250193. Available from: https://doi.org/10.1142/S0217979222501934.

[13] Durmus SA. Optical soliton solutions of stochastic the third order nonlinear Schrödinger equation with multiplicative white noise via Itô calculus. *Optical and Quantum Electronics*. 2024; 56: 779. Available from: https://doi.org/10.1007/s11082-024-06413-8.

[14] Ozdemira N, Altunb S, Ozisikc M, Secerd A, Bayrame M. Bright soliton of stochastic perturbed Biswas-Milovic equation with cubic-quintic-septic law having multiplicative white noise. *Mexican Journal of Physics*. 2024; 70: 021303. Available from: https://doi.org/10.31349/revmexfis.70.021303.

[15] Abdelrahman ME, Mohammed WW, Alesemi M, Albosaily S. The effect of multiplicative noise on the exact solutions of nonlinear Schrödinger equation. *AIMS Mathematics*. 2021; 6(1): 2970-2980. Available from: https://doi.org/10.3934/math.2021180.

[16] Albosaily S, Mohammed WW, Aiyashi MA, Abdelrahman MAE. Exact solutions of the (2 + 1)-dimensional stochastic chiral nonlinear Schrödinger equation. *Symmetry*. 2020; 12(11): 1874. Available from: https://doi.org/10.3390/sym12111874.

[17] Jawad AJM, Abu-AlShaeer MJ. Highly dispersive optical solitons with cubic law and cubic-quintic-septic law nonlinearities by two methods. *Al-Rafidain Journal of Engineering Sciences*. 2023; 1(1): 1-8. Available from: https://doi.org/10.61268/sapgh524.

[18] Jihad N, Almuhsan MAA. Evaluation of impairment mitigations for optical fiber communications using dispersion compensation techniques. *Al-Rafidain Journal of Engineering Sciences*. 2023; 1(1): 81-92. Available from: https://doi.org/10.61268/0dat0751.

[19] Dakova-Mollova A, Miteva P, Slavchev V, Kovachev K, Kasapeteva Z, Dakova D, et al. Propagation of broad-band optical pulses in dispersionless media. *Ukrainian Journal of Physical Optics*. 2024; 25(5): S1102-S1110. Available from: https://doi.org/10.3116/16091833/Ukr.J.Phys.Opt.2024.S1102.

[20] Polyanin AD, Kudryashov NA. Nonlinear Schrödinger equations with delay: closed-form and generalized separable solutions. *Contemporary Mathematics*. 2024; 5(4): 5783-5794. Available from: https://doi.org/10.37256/cm.5420245840.

[21] Mendez-Zuniga IM, Belyaeva TL, Agüero MA, Serkin VN. Multisoliton bound states in the fourth-order concatenation model of the nonlinear Schrödinger equation hierarchy. *Transactions in Optics and Photonics*. 2025; 1(1): 22-33.

[22] Sarkar RK, Dutta MK. Dissimilar types of joined propagation of two beams in a holographic medium. *Journal of Optics*. 2024. Available from: https://doi.org/10.1007/s12596-024-02288-w.

[23] Raza A, Kara AH, Alqurashi BM. Double reduction via invariance & conservation laws and analysis of solitons of the Gerdjikov-Ivanov equation in optics. *Journal of Optics*. 2024. Available from: https://doi.org/10.1007/s12596-024-02193-2.

[24] Murad MAS. Formation of optical soliton wave profiles of nonlinear conformable Schrödinger equation in weakly non-local media: Kudryashov auxiliary equation method. *Journal of Optics*. 2024. Available from: https://doi.org/10.1007/s12596-024-02110-7.

[25] Ma WX. Lump solutions to the Kadomtsev-Petviashvili equation. *Physics Letters A*. 2015; 379(36): 1975-1978. Available from: https://doi.org/10.1016/j.physleta.2015.06.061.

[26] Aceves AB, Wabnitz S. Self-induced transparency solitons in nonlinear refractive periodic media. *Physics Letters A*. 1989; 141: 37-42. Available from: https://doi.org/10.1016/0375-9601(89)90441-6.

[27] De Sterke CM, Sipe JE. Gap solitons. *Progress in Optics*. 1994; 33: 203-260.

[28] Zayed EME, Alngar MEM, Shohib RMA, Gepreel KA, Nofal TA. Optical solitons with $(2+1)$-dimensional nonlinear Schrödinger equation having spatio-temporal dispersion and multiplicative white noise via Itô calculus. *Optik*. 2022; 261: 169204. Available from: https://doi.org/10.1016/j.ijleo.2022.169204.

[29] Zayed EME, Shohib RMA, Alngar MEM. Dispersive optical solitons in birefringent fibers for $(2+1)$-dimensional NLSE with Kerr-law nonlinearity and spatio-temporal dispersion having multiplicative white noise via Itô calculus. *Optik*. 2022; 267: 169667. Available from: https://doi.org/10.1016/j.ijleo.2022.169667.

[30] Wang K-J, Liu J-H. On abundant wave structures of the unsteady Korteweg-de Vries equation arising in shallow water. *Journal of Ocean Engineering and Science*. 2023; 8(6): 595-601. Available from: https://doi.org/10.1016/j.joes.2022.04.024.

[31] Wang K-J, Shi F, Liu J-H. Soliton molecules and the novel hybrid interaction solutions of the new extended $(3+1)$-dimensional Boiti-Leon-Manna-Pempinelli equation. *Pramana-Journal of Physics*. 2024; 98: 67. Available from: https://doi.org/10.1007/s12043-024-02747-w.

[32] Wang K-J. The perturbed Chen-Lee-Liu equation: Diverse optical soliton solutions and other wave solutions. *Advances in Mathematical Physics*. 2024; 4990396. Available from: https://doi.org/10.1155/2024/4990396.

[33] Wang K-J. Resonant multiple wave, periodic wave and interaction solutions of the new extended $(3+1)$-dimensional Boiti-Leon-Manna-Pempinelli equation. *Nonlinear Dynamics*. 2023; 111: 16427-16439. Available from: https://doi.org/10.1007/s11071-023-08699-x.

[34] Wang K-J. Diverse wave structures to the modified Benjamin-Bona-Mahony equation in the optical illusions field. *Modern Physics Letters B*. 2023; 37(11): 2350012. Available from: https://doi.org/10.1142/S0217984923500124.

[35] Wang K-J, Zou B-R, Zhu H-W, Li S, Li G. Phase portrait, bifurcation and chaotic analysis, variational principle, hamiltonian, novel solitary, and periodic wave solutions of the new extended korteweg-de vries-type equation. *Mathematical Methods in the Applied Sciences*. 2025; 48(9): 9901-9909. Available from: https://doi.org/10.1002/mma.10852.

[36] Wang K-J. A fast insight into the optical solitons of the generalized third-order nonlinear Schrödinger's equation. *Results in Physics*. 2022; 40: 105872. Available from: https://doi.org/10.1016/j.rinp.2022.105872.

[37] Wang K-J. He's variational method for the time-space fractional nonlinear Drinfeld-Sokolov-Wilson system. *Mathematical Methods in the Applied Sciences*. 2023; 46: 7798-7806. Available from: https://doi.org/10.1002/mma.7200.